PHOTONICS Research

Gap solitons in parity–time symmetric moiré optical lattices

Xiuye Liu[1,2] and Jianhua Zeng[1,2,*]

[1]State Key Laboratory of Transient Optics and Photonics, Xi'an Institute of Optics and Precision Mechanics of Chinese Academy of Sciences, Xi'an 710119, China
[2]University of Chinese Academy of Sciences, Beijing 100049, China
*Corresponding author: zengjh@opt.ac.cn

Received 31 August 2022; revised 2 December 2022; accepted 4 December 2022; posted 6 December 2022 (Doc. ID 474527); published 23 January 2023

Parity–time ($\mathcal{PT}$) symmetric lattices have been widely studied in controlling the flow of waves, and recently, moiré superlattices, connecting the periodic and non-periodic potentials, have been introduced for exploring unconventional physical properties in physics, while the combination of both and nonlinear waves therein remains unclear. Here, we report a theoretical survey of nonlinear wave localizations in $\mathcal{PT}$ symmetric moiré optical lattices, with the aim of revealing localized gap modes of different types and their stabilization mechanism. We uncover the formation, properties, and dynamics of fundamental and higher-order gap solitons as well as vortical ones with topological charge, all residing in the finite bandgaps of the underlying linear-Bloch wave spectrum. The stability regions of localized gap modes are inspected in two numerical ways: linear-stability analysis and direct perturbance simulations. Our results provide an insightful understanding of soliton physics in combined versatile platforms of $\mathcal{PT}$ symmetric systems and moiré patterns.

https://doi.org/10.1364/PRJ.474527

1. INTRODUCTION

The moiré pattern—a periodic pattern overlapping its copy with a relative twist—as a novel two-dimensional (2D) material has shown great unique physical properties in condensed matter physics, including tunable flatbands, superconductivity, and correlated insulator phases at twist (magic) angles in twisted double-layer graphene [1–4], leading to an emerging field called twistronics—manipulating electronic properties through the relative twist angle [5]. Recently, the studies of moiré patterns and physics have entered regimes of optics and photonics: particularly, reconfigurable photonic moiré lattices were created in 2D photorefractive media by optical induction [6], and localization–delocalization transition of light [7] and optical soliton formation induced by the twisting angle [8,9] were observed, respectively, in linear and nonlinear contexts; magic-angle lasers with unique confinement mechanisms were fabricated in nanostructured moiré superlattices [10]; and multifrequency soliton generation in quadratic nonlinear media with commensurate–incommensurate photonic moiré lattices was predicted [11], to name just a few examples.

In addition, moiré optical lattices have been proposed in the context of ultracold atoms, and the associated moiré physics therein is being revealed [12–14]. To be specific, simulating twisted bilayers is possible by using cold atoms in state-dependent optical lattices that show Dirac-like physics and a band narrowing feature, making them ideal candidates to observe similar physics (such as strongly correlated phenomena in condensed matters) with larger rotation angles [12]. Simulating twistronics without a twist, a highly tunable scheme that rules out a physical bilayer or twist to synthetically emulate twisted bilayer systems in the setting of ultracold atoms trapped in an optical lattice, was proposed [13]. Moiré physics including tunable flatbands and Larkin–Ovchinnikov superfluids in spin-twisted optical lattices (rather than bilayers) was investigated [14], and considering that electromagnetically induced regular optical (or photonic) lattices via atomic coherence in atomic ensembles are mature in experiments, we recently proposed a related scheme to create electromagnetically induced moiré optical lattices in a three-level coherent atomic gas (either hot or cold atoms) in the regime of electromagnetically induced transparency [15]. Consequently, we can safely conclude that optics and ultracold atoms open flexible and promising routes toward the realization of moiré optical lattices and associated moiré physics.

Moiré patterns bridge the gap between periodic structures and aperiodic ones, offering a new platform for studying nonlinear localization of light [8,9]. Particularly, conventional periodic structures such as photonic crystals and lattices in optics [16–18] and optical lattices in the context of ultracold atoms [19–21] exhibit finite photonic or atomic bandgaps [22], the precise control of which and the corresponding nonlinearity

could result in the emergence of a new spatially self-localized state called gap solitons (GSs) under repulsive (defocusing) nonlinearity [23–32]. Experimentally, optical GSs have been confirmed in optical Bragg gratings [33] and nonlinear photonic crystals [34], and the creation of atomic GSs of Bose–Einstein condensates (BECs) in optical lattices [35]. It is worth noting that parity–time ($\mathcal{PT}$) symmetric lattices as an interesting periodic structure were heavily studied in optical [36–41] and matter-wave [42,43] media and beyond in past years, providing a fertile land for investigating nonlinear waves including GSs [44–49]. However, to the best of our knowledge, the combination of moiré patterns and $\mathcal{PT}$ symmetry has not yet been reported.

In this work, we address the formation, properties, and dynamical stability of matter-wave GSs in a BEC trapped with $\mathcal{PT}$ symmetric moiré optical lattices constituted of two 2D $\mathcal{PT}$ lattices with a twist (rotation) angle. Spatially localized nonlinear excitations of three kinds of coherent matter waves—fundamental GSs and high-order ones grouped as two fundamental modes, as well as gap vortices with topological charge—situated inside the first and second atomic bandgaps of the linear Bloch-wave spectrum are found, underlining the tunable flatbands of the twisting $\mathcal{PT}$ periodic structure and robust stability of the reconfigurable nonlinear localized matter-wave structures within the associated gaps. The stability and instability properties of the nonlinear localized modes are assessed by linear-stability analysis and direct perturbance simulations, and both show good agreement.

2. RESULTS AND DISCUSSION

A. Theoretical Model

1. Gross–Pitaevskii Equation

The dynamics of a BEC cloud in 2D $\mathcal{PT}$ symmetric moiré optical lattices is described by the Gross–Pitaevskii (GP) equation for the dimensionless macroscopic wave function Ψ [19–21,49,50]:

$$i\frac{\partial\Psi}{\partial t} = -\frac{1}{2}\nabla^2\Psi + V_{\mathcal{PT}}(\mathbf{r})\Psi + |\Psi|^2\Psi, \tag{1}$$

where Laplacian $\nabla^2 = \partial^2/\partial x^2 + \partial^2/\partial y^2$, and $\mathbf{r} = (x, y)$; the last term represents the nonlinearity where the repulsive atom–atom interaction controlled by Feshbach resonance is chosen. We stress that in the context of nonlinear optics, the corresponding nonlinear Schrödinger equation for the propagation dynamics of field amplitude is deduced readily by substituting the time t with propagation distance z in Eq. (1). The $\mathcal{PT}$ moiré lattice under study yields

$$V_{\mathcal{PT}}(\mathbf{r}) = V_1[(\cos^2 x + \cos^2 y) + iV_0(\sin 2x + \sin 2y)] + V_2[(\cos^2 x' + \cos^2 y') + iV_0(\sin 2x' + \sin 2y')], \tag{2}$$

where $V_{1,2}$ is the strength, V_0 is the imaginary potential strength, and the strength contrast between the two sublattices is defined as $p = V_2/V_1$, setting $V_1 = 4$ for discussion. Note that the potential Eq. (2) matches the requirement of $\mathcal{PT}$ symmetry, $V_{\mathcal{PT}}(\mathbf{r}) = V^*_{\mathcal{PT}}(-\mathbf{r})$, and it reduces to the usual (non-$\mathcal{PT}$) moiré lattice at $V_0 = 0$, and to the conventional $\mathcal{PT}$ lattice at $V_2 = 0$. The (x, y) plane is related to the rotation (x', y') plane with a twisting angle θ:

$$\begin{pmatrix} x' \\ y' \end{pmatrix} = \begin{pmatrix} \cos\theta & -\sin\theta \\ \sin\theta & \cos\theta \end{pmatrix}\begin{pmatrix} x \\ y \end{pmatrix}. \tag{3}$$

2. Linear Tunable Flatband Properties

Depicted in Fig. 1 is the linear Bloch spectrum of the $\mathcal{PT}$ moiré optical lattice [Eq. (2)] under Pythagorean angle $\theta = \arctan[2\alpha\beta/(\alpha^2 - \beta^2)]$, with the Pythagorean triples $(\alpha^2 - \beta^2, 2\alpha\beta, \alpha^2 + \beta^2)$ for natural numbers (α, β). One can see from Fig. 1(a) that the widths of the first and second finite gaps compress rapidly with increasing V_0 at a defined angle θ [i.e., $\theta = \arctan(3/4)$], and non-Hermitian degeneracy arises at an exceptional point (singularity) $V_0 = 0.5$, at which there is no Bloch gap. With an increase of strength contrast p, more and more flatbands appear, widening the first gap while splitting the second gap, according to Fig. 1(b). For the 2D square $\mathcal{PT}$ moiré lattice at Pythagorean angle, the associated first reduced Brillouin zone in reciprocal space is given in Fig. 1(c). Typical real and imaginary parts of such lattices are shown in Figs. 1(d) and 1(e) at $\theta = \arctan(3/4)$, and in Figs. 1(g) and 1(h) at $\theta = \arctan(5/12)$; the corresponding linear bandgap structures are respectively shown in Figs. 1(f) and 1(i), where there are broad first and second gaps.

The stationary solution ϕ at chemical potential μ of Eq. (1) is given by $\Psi = \phi e^{-i\mu t}$ (or $\Psi = \phi e^{i\mu t}$ with μ the propagation constant, in the context of nonlinear optics), yielding

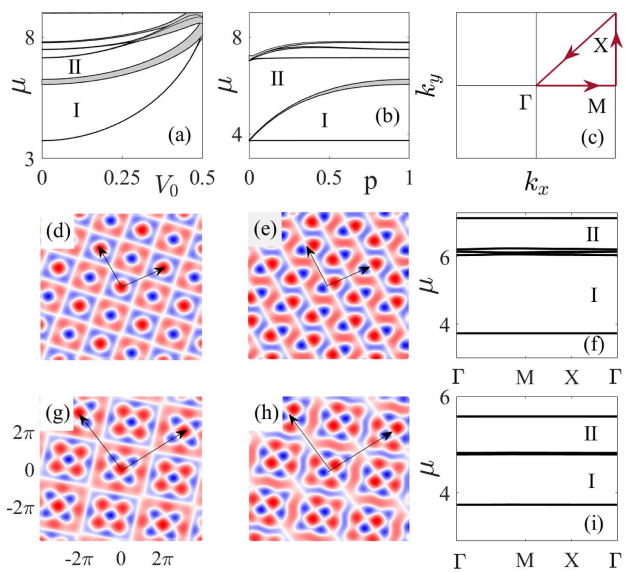

Fig. 1. Bandgap structures for 2D $\mathcal{PT}$ symmetric moiré optical lattices at $\theta = \arctan(3/4)$ with increasing imaginary potential strength V_0 (a) and strength contrast p (b). (c) First Brillouin zone in 2D reciprocal space. Contour plots of the real (d), (g) and imaginary (e), (h) parts of the lattice (blue, lattice potential minima; red, lattice potential maxima) at $\theta = \arctan(3/4)$ (d), (e) and $\theta = \arctan(5/12)$ (g), (h), and their corresponding bandgap diagrams (f), (i) at $V_0 = 0.02$ and $p = 1$ in reduced zone representation. I and II in (f), (i) represent the first and second bandgaps.

$$\mu\phi = -\frac{1}{2}\nabla^2\phi + V_{\mathcal{PT}}(\mathbf{r})\phi + |\phi|^2\phi. \quad (4)$$

Since we are interested in GS solutions supported by 2D $\mathcal{PT}$ moiré lattices, their stability property is a key issue, which is evaluated by linear-stability analysis. Thus, we perturb the solution as $\psi = [\Phi + \rho\exp(\lambda t) + \varrho^*\exp(\lambda^* t)]\exp(-i\mu t)$, where Φ is the unperturbed solution constructed from Eq. (4), and ρ and ϱ are small perturbations under eigenvalue λ. Substituting it into Eq. (1) would lead to the linear eigenvalue problem:

$$i\lambda\rho = -\frac{1}{2}\nabla^2\rho - \mu\rho + V_{\mathcal{PT}}(\mathbf{r})\rho + 2|\phi|^2\rho + \phi^2\varrho, \quad (5)$$

$$i\lambda\varrho = +\frac{1}{2}\nabla^2\varrho + \mu\varrho - V^*_{\mathcal{PT}}(\mathbf{r})\varrho - 2|\phi|^2\varrho - \phi^2\rho. \quad (6)$$

One can see from Eqs. (5) and (6) that the solution is stable only when all real parts of the eigenvalues are zero [$\mathrm{Re}(\lambda) = 0$]; it is unstable otherwise.

B. Nonlinear Localized Modes and Their Properties

1. Fundamental Gap Solitons

The typical nonlinear localized mode in $\mathcal{PT}$ moiré optical lattices is the fundamental mode, matter-wave GSs, populated within atomic finite gaps, the characteristic profile of which is displayed in Figs. 2(a)–2(c). It is observed that the real wave function, $\mathrm{Re}(\phi)$, resembles a bright GS, while its imaginary part, $\mathrm{Im}(\phi)$, takes the form of a dipole. The condensate population, which is the number of atoms, $N = \int_{-\infty}^{+\infty}|\phi(\mathbf{r})|^2 d\mathbf{r}$, as a function of the chemical potential μ for GSs in $\mathcal{PT}$ moiré lattices at $\theta = \arctan(3/4)$, is shown in Fig. 2(d), displaying an "anti-Vakhitov–Kolokolov" (anti-VK) criterion, $dN/d\mu > 0$, a necessary but not sufficient condition for the stability of GSs in periodic structures with repulsive (defocusing) nonlinearity [29–32]. For a given μ inside the first gap, the dependency between number of atoms N and strength contrast p, $N(p)$, is obtained in Fig. 2(e), revealing a slight vibration of N when altering p; such a feature provides a flexible opportunity to launch fundamental GSs in moiré optical lattices with changeable strength contrasts, in addition to the twisting angle θ. Figure 2(f) depicts N versus imaginary potential strength V_0 at $\theta = \arctan(3/4)$ and $\mu = 6.7$ (within the second finite gap), showing a decrease tendency. We emphasize that the fundamental GSs are very stable in the midst of the first and second gaps; they are unstable as long as they are excited near both edges of the Bloch bands, and the directly perturbed evolutions shown in the following will prove it.

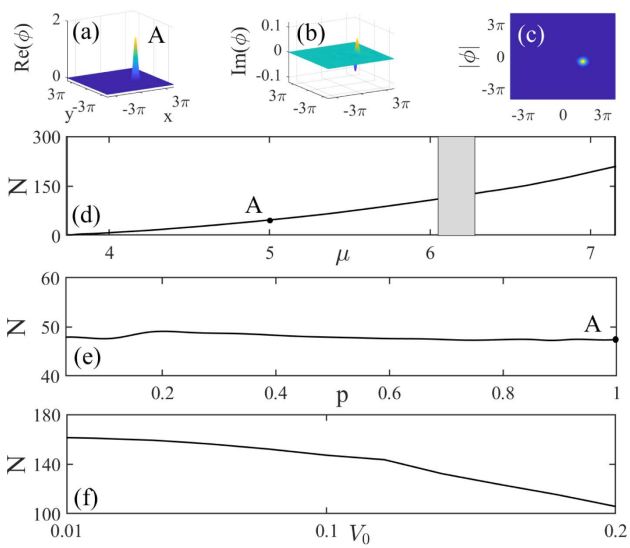

Fig. 2. Typical profile of a fundamental GS supported by the 2D $\mathcal{PT}$ symmetric moiré optical lattice at $\theta = \arctan(3/4)$ (a)–(c). Corresponding real (a) and imaginary (b) parts, and contour plot of the module (c). Condensate population, N, as a function of chemical potential μ (d), strength contrast p (e), and imaginary potential strength V_0 (f) at $\theta = \arctan(3/4)$. Other parameters: $\mu = 5$, $N = 47.4$ in (a)–(c). $\mu = 6.7$ in (f).

2. Higher-Order Gap Solitons

Besides the fundamental mode reported in Fig. 2, $\mathcal{PT}$ moiré optical lattices can also support higher-order spatially localized gap modes that may be considered as composite structures of several fundamental GSs. Two examples of such higher-order modes, composed of two out-of-phase and in-phase fundamental GSs, are displayed in Figs. 3(a), 3(b) and Figs. 3(c), 3(d), respectively. Their contour plots are shown in the second line of Fig. 3, with an emphasis on their tilted placements structured by twisting optical lattices; conforming to the fundamental counterpart in Fig. 2(b), the imaginary sections of the composite GSs emerge always as a dipole mode. The depending relations $N(\mu)$ of both higher-order GS modes are summed up in Fig. 3(i), demonstrating, once again, the empirical stability of anti-VK criterion $dN/d\mu > 0$ [29–32].

3. Gap Vortices

It is instructive to see whether $\mathcal{PT}$ moiré optical lattices can sustain robust stable complex localized gap modes represented as gap vortices with topological charge (winding number) S. Our numerical calculations demonstrate that it is possible to create stable gap vortices with $S = 1$ in such a novel periodic structure, provided that they are excited within finite gaps. Typical profiles of 2D hollow gap vortices with $S = 1$ are in the form of four fundamental GSs entangled with 2π phase, according to Figs. 4(a) and 4(b), where the corresponding real and imaginary parts of the wave functions and the associated phase structures are included. Evidently, both real and imaginary parts show the similarity of having positive and negative values; and counterintuitively, the imaginary wave function $\mathrm{Im}(\phi)$ for the vortex gap mode does not exhibit a dipole-like feature for each fundamental GS, in contrast to their fundamental counterparts and higher-order ones as depicted in Fig. 2(b) and Figs. 3(b), 3(d), 3(f), and 3(h). The non-dipole feature of the imaginary parts of the gap vortices may be explained by the unique and inherent property of localized vortical modes—the phase factor, which, together with the structural property of $\mathcal{PT}$ moiré optical lattices, determines the wave structures (both real and imaginary parts) of gap vortices. This can be clearly observed from the corresponding phase structures of the gap vortices displayed in the right columns of the first two lines of Fig. 4. Also, in Fig. 4(c), we obtain the curve $N(\mu)$ for such kinds of gap vortices with topological charge $S = 1$, showing an increase relationship.

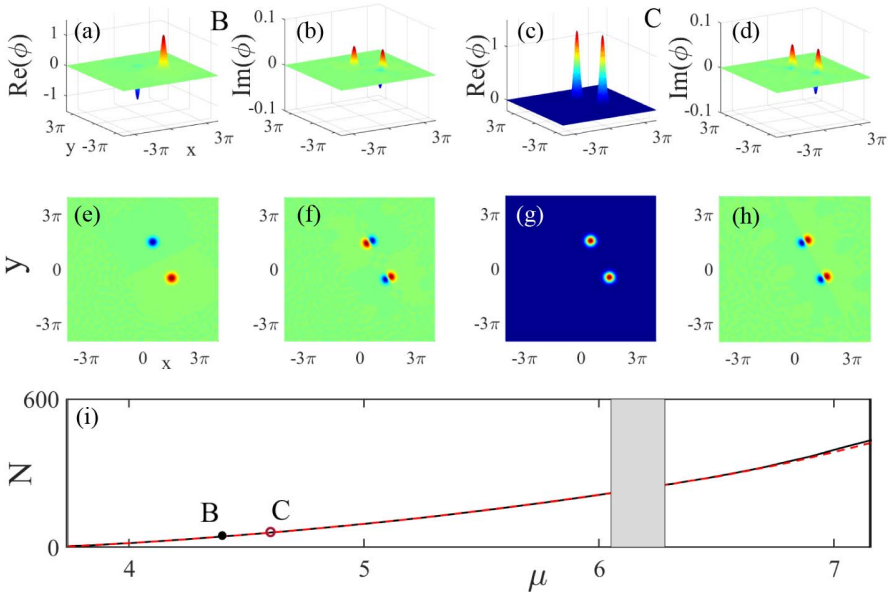

Fig. 3. Typical profiles of higher-order GSs grouped as two out-of-phase (a), (b) and in-phase (c), (d) fundamental GSs at $\theta = \arctan(3/4)$; corresponding contour plots are displayed in the second line (e)–(h). (i) Condensate population, N, as a function of chemical potential μ at $\theta = \arctan(3/4)$ (black, out-of-phase mode; red dashed, in-phase mode). Other parameters: $\mu = 4.4$, $N = 43.9$ for B and $\mu = 4.6$, $N = 59.3$ for C.

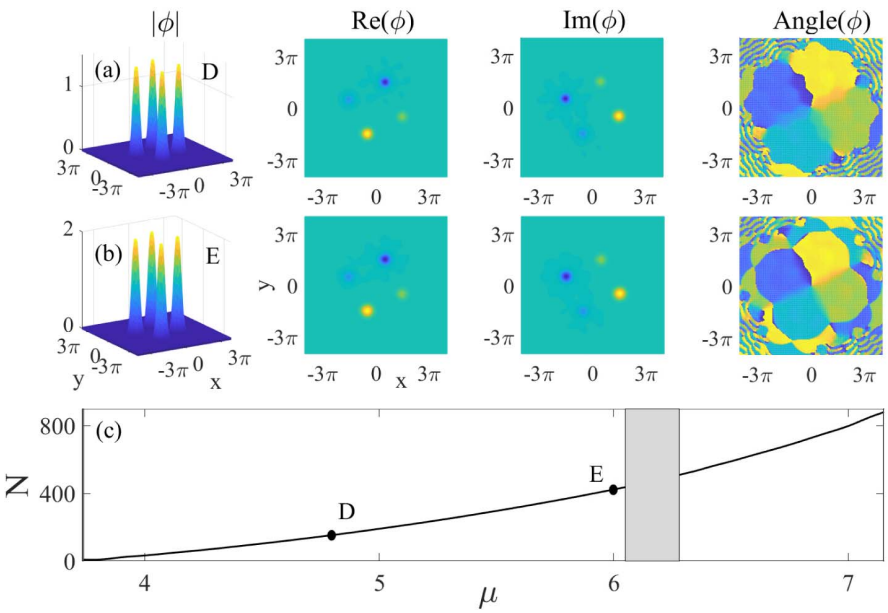

Fig. 4. Profiles of gap vortices consisting of four fundamental GSs with vortex charge $S = 1$ prepared within (a) and near the upper edge (b) of the first finite gap; corresponding condensate population, N, as a function of chemical potential μ at $\theta = \arctan(3/4)$ (c). Panels for the top and center lines denote, respectively, contour plot of the module, real and imaginary parts, as well as the associated phase structure. Other parameters for gap vortices marked by points D and E: (a) $\mu = 4.8$, $N = 153.5$; (b) $\mu = 6$, $N = 430$.

4. Dynamics of Gap Solitons and Vortices

The stability properties of all 2D localized gap modes (fundamental and higher-order GSs, gap vortices) have been measured in linear-stability analysis and direct numerical simulations of the perturbed evolutions, using Eqs. (5), (6), and (1), as pointed out previously. Our findings suggest the common feature of spatially localized modes supported by $\mathcal{PT}$ moiré periodic structures, that is, the GSs, is stable within the middle portions of finite gaps and unstable close to the band edges. For the fundamental GSs in Figs. 5(a) and 5(b), higher-order modes in Figs. 5(c) and 5(d), and gap vortices at topological charge $S = 1$ in Figs. 5(e) and 5(f), with the stable ones being

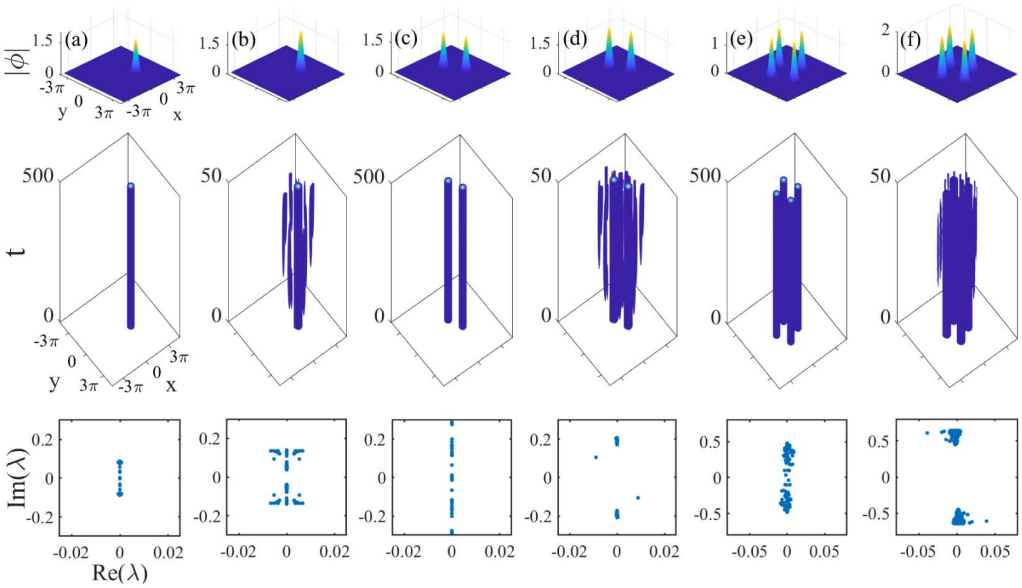

Fig. 5. Profiles of fundamental GSs (a), (b), higher-order GSs (c), (d), and gap vortices with $S = 1$ (e), (f) prepared within the first (a), (c), (e), (f) and second (b), (d) finite gaps. Corresponding perturbed evolutions and linear eigenvalue spectra obtained from linear-stability analysis are displayed in the second and third lines, respectively. Other parameters: (a) $\mu = 5$, $N = 47.4$; (b) $\mu = 6.29$, $N = 128.2$; (c) $\mu = 5.2$, $N = 114.7$; (d) $\mu = 6.28$, $N = 252.6$; (e) $\mu = 4.8$, $N = 153.5$; (f) $\mu = 6$, $N = 430$. White noise with 10% of its soliton's amplitude is applied for all.

prepared in gaps and unstable ones near the band edges, their directly perturbed evolutions are depicted in the second line of Fig. 5, which are in good agreement with their linear eigenvalue spectra produced by linear-stability analysis in the bottom line of Fig. 5. It is important to emphasize that during evolution, the unstable localized gap modes develop multiple side peaks that reduce the necessary number of atoms (N) for sustaining the original gap modes; by contrast, shapes (good coherence) of stable modes can always remain. It must be pointed that the real eigenvalues in Figs. 5(a), 5(c), and 5(e) for stable GSs are not exactly zero, because we use the truncated matrix limited by our insufficient memory and CPU power, confirming the requirement of large spatial grid points in dealing with moiré optical lattices (compared to that with conventional ones).

5. Stability Regions for Stable Localized Gap Modes

Before proceeding to the next section, we stress that the stability regions of all the localized gap modes considered above are accumulated in Table 1. It is seen that there are wide stable regions within the first two finite gaps, no matter what kind of localized gap mode, providing compelling evidence that localized gap modes are robust enough in moiré optical lattices with flatbands. Another common feature of all these localized modes is that they are always populated at the lattice potential minima, which change with the change of the twist angle-dependent lattice structure.

Table 1. Stability Regions (Characterized by μ) of Nonlinear Localized Modes within the First and Second Finite Gaps

Localized Modes	Stability Regions (μ)
Fundamental gap solitons	$3.74 \le \mu \le 6$ and $6.7 \le \mu \le 7.1$
Out-of-phase gap solitons	$3.74 \le \mu \le 5.95$ and $6.8 \le \mu \le 7.1$
In-phase gap solitons	$3.74 \le \mu \le 5.95$ and $6.8 \le \mu \le 7.1$
Gap vortices	$3.74 \le \mu \le 5.9$ and $6.9 \le \mu \le 7.0$

C. Experimental Consideration

Although our focus is merely on BECs loaded onto $\mathcal{PT}$ moiré optical lattices, the physical system under study could directly apply to the nonlinear optics context for describing light propagation in $\mathcal{PT}$ moiré photonic crystals and lattices, since both contexts share the same model [51]. The only difference is to replace the time t by propagation direction z in Eq. (1), and the chemical potential μ by propagation constant $-b$ in Eq. (4); then the wave function $\phi(x, t)$ is replaced by the electromagnetic field amplitude of laser pulse $E(z, x)$, and the number of atoms N would be the soliton power U. Considering the fact that $\mathcal{PT}$ optical lattices have been successfully fabricated in optics (and photonics) [36–41] and ultracold atoms [42,43], the $\mathcal{PT}$ optical lattices of moiré type could also be practically realized using current-state-of-the-art experimental technologies. Specifically, this is achievable in optics using optical waveguides of semiconductor structure with alternating $\mathcal{PT}$-symmetric gain–loss modulation [52] or distributed-feedback optical structures with gain or loss regions [53]. In terms of atomic gases, this is accomplishable in a gas of multilevel atoms such as the ^{85}Rb atomic system working under electromagnetically induced transparency [15,42,43]. Particularly, GSs have been created in both contexts [33–35], and the spatially localized gap modes predicted here can thus be envisioned in both experimental platforms.

D. Materials and Methods

All the numerical results presented above obey the following numerical procedure: the stationary GS solution is first found

from Eq. (4) via a modified squared-operator iteration method [54]; then its stability is measured by means of the linear-stability analysis [Eqs. (5) and (6)] in the Fourier collocation method [54], and direct perturbance simulations [Eq. (1)] using the fourth-order Runge–Kutta method in real time.

3. CONCLUSION

We have addressed an as yet unresolved issue of the excitations and stability of 2D GSs supported by $\mathcal{PT}$ symmetric moiré optical lattices that exhibit a tunable flatband feature. Three categories of GSs are found, which are fundamental GSs and higher-order ones as well as gap vortices with topological charge, residing in both the first and second finite bandgaps of the associated diffraction diagram, and their stability is evaluated in linear-stability analysis and direct perturbance simulations. The experimental platforms for observing them are discussed, and we envision that the localized gap modes in $\mathcal{PT}$ symmetric moiré periodic structures are within reach in contexts of nonlinear optics and atomic media.

Funding. National Natural Science Foundation of China (12074423, 61690222, 61690224); Young Scholars of Chinese Academy of Sciences in Western China Program (XAB2021YN18).

Disclosures. The authors declare no conflicts of interest.

Data Availability. No data were generated or analyzed in the presented research.

REFERENCES

1. R. Bistritzer and A. H. MacDonald, "Moiré bands in twisted double-layer graphene," Proc. Natl. Acad. Sci. USA **108**, 12233–12237 (2011).
2. Y. Cao, V. Fatemi, S. Fang, K. Watanabe, T. Taniguchi, E. Kaxiras, and P. Jarillo-Herrero, "Unconventional superconductivity in magic-angle graphene superlattices," Nature **556**, 43–50 (2018).
3. Y. Cao, V. Fatemi, A. Demir, S. Fang, S. L. Tomarken, J. Y. Luo, J. D. Sanchez-Yamagishi, K. Watanabe, T. Taniguchi, E. Kaxiras, R. C. Ashoori, and P. Jarillo-Herrero, "Correlated insulator behaviour at half-filling in magic-angle graphene superlattices," Nature **556**, 80–84 (2018).
4. G. W. Burg, J. Zhu, T. Taniguchi, K. Watanabe, A. H. MacDonald, and E. Tutuc, "Correlated insulating states in twisted double bilayer graphene," Phys. Rev. Lett. **123**, 197702 (2019).
5. S. Carr, D. Massatt, S. Fang, P. Cazeaux, M. Luskin, and E. Kaxiras, "Twistronics: manipulating the electronic properties of two-dimensional layered structures through their twist angle," Phys. Rev. B **95**, 075420 (2017).
6. J. W. Fleischer, M. Segev, N. K. Efremidis, and D. N. Christodoulides, "Observation of two-dimensional discrete solitons in optically induced nonlinear photonic lattices," Nature **422**, 147–150 (2003).
7. P. Wang, Y. Zheng, X. Chen, C. Huang, Y. V. Kartashov, L. Torner, V. V. Konotop, and F. Ye, "Localization and delocalization of light in photonic moiré lattices," Nature **577**, 42–46 (2020).
8. Q. Fu, P. Wang, C. Huang, Y. V. Kartashov, L. Torner, V. V. Konotop, and F. Ye, "Optical soliton formation controlled by angle twisting in photonic moiré lattices," Nat. Photonics **14**, 663–668 (2020).
9. C. Huang, F. Ye, X. Chen, Y. V. Kartashov, V. V. Konotop, and L. Torner, "Localization-delocalization wavepacket transition in Pythagorean aperiodic potentials," Sci. Rep. **6**, 32546 (2016).
10. X.-R. Mao, Z.-K. Shao, H.-Y. Luan, S.-L. Wang, and R.-M. Ma, "Magic-angle lasers in nanostructured moiré superlattice," Nat. Nanotechnol. **16**, 1099–1105 (2021).
11. Y. V. Kartashov, F. Ye, V. V. Konotop, and L. Torner, "Multifrequency solitons in commensurate-incommensurate photonic moiré lattices," Phys. Rev. Lett. **127**, 163902 (2021).
12. A. González-Tudela and J. I. Cirac, "Cold atoms in twisted-bilayer optical potentials," Phys. Rev. A **100**, 053604 (2019).
13. T. Salamon, A. Celi, R. W. Chhajlany, I. Frérot, M. Lewenstein, L. Tarruell, and D. Rakshit, "Simulating twistronics without a twist," Phys. Rev. Lett. **125**, 030504 (2020).
14. X.-W. Luo and C. Zhang, "Spin-twisted optical lattices: tunable flat bands and Larkin-Ovchinnikov superfluids," Phys. Rev. Lett. **126**, 103201 (2021).
15. Z. Chen, X. Liu, and J. Zeng, "Electromagnetically induced moiré optical lattices in a coherent atomic gas," Front. Phys. **17**, 42508 (2022).
16. Y. S. Kivshar and G. P. Agrawal, *Optical Solitons: From Fibers to Photonic Crystals* (Academic, 2003).
17. J. D. Joannopoulos, S. G. Johnson, J. N. Winn, and R. D. Meade, *Photonic Crystals: Molding the Flow of Light*, 2nd ed. (Princeton University, 2011).
18. I. L. Garanovich, S. Longhi, A. A. Sukhorukova, and Y. S. Kivshar, "Light propagation and localization in modulated photonic lattices and waveguides," Phys. Rep. **518**, 1–79 (2012).
19. O. Morsch and M. Oberthaler, "Dynamics of Bose-Einstein condensates in optical lattices," Rev. Mod. Phys. **78**, 179–215 (2006).
20. Y. V. Kartashov, B. A. Malomed, and L. Torner, "Solitons in nonlinear lattices," Rev. Mod. Phys. **83**, 247–305 (2011).
21. Y. V. Kartashov, G. E. Astrakharchik, B. A. Malomed, and L. Torner, "Frontiers in multidimensional self-trapping of nonlinear fields and matter," Nat. Rev. Phys. **1**, 185–197 (2019).
22. I. H. Deutsch, R. J. C. Spreeuw, S. L. Rolston, and W. D. Phillips, "Photonic band gaps in optical lattices," Phys. Rev. A **52**, 1394–1410 (1995).
23. W. Chen and D. L. Mills, "Gap solitons and the nonlinear optical response of superlattices," Phys. Rev. Lett. **58**, 160–163 (1987).
24. S. John and N. Aközbek, "Nonlinear optical solitary waves in a photonic band gap," Phys. Rev. Lett. **71**, 1168–1171 (1993).
25. A. Kozhekin and G. Kurizki, "Self-induced transparency in Bragg reflectors: gap solitons near absorption resonances," Phys. Rev. Lett. **74**, 5020–5023 (1995).
26. A. E. Kozhekin, G. Kurizki, and B. Malomed, "Standing and moving gap solitons in resonantly absorbing gratings," Phys. Rev. Lett. **81**, 3647–3650 (1998).
27. Y. Zhang and B. Wu, "Composition relation between gap solitons and Bloch waves in nonlinear periodic systems," Phys. Rev. Lett. **102**, 093905 (2009).
28. E. A. Ostrovskaya and Y. S. Kivshar, "Matter-wave gap solitons in atomic band-gap structures," Phys. Rev. Lett. **90**, 160407 (2003).
29. L. Zeng and J. Zeng, "Gap-type dark localized modes in a Bose-Einstein condensate with optical lattices," Adv. Photon. **1**, 046004 (2019).
30. J. Shi and J. Zeng, "Self-trapped spatially localized states in combined linear-nonlinear periodic potentials," Front. Phys. **15**, 12602 (2020).
31. J. Li and J. Zeng, "Dark matter-wave gap solitons in dense ultracold atoms trapped by a one-dimensional optical lattice," Phys. Rev. A **103**, 013320 (2021).
32. J. Chen and J. Zeng, "Dark matter-wave gap solitons of Bose-Einstein condensates trapped in optical lattices with competing cubic-quintic nonlinearities," Chaos Solitons Fractals **150**, 111149 (2021).
33. B. J. Eggleton, R. E. Slusher, C. M. de Sterke, P. A. Krug, and J. E. Sipe, "Bragg grating solitons," Phys. Rev. Lett. **76**, 1627–1630 (1996).
34. D. Mandelik, R. Morandotti, J. S. Aitchison, and Y. Silberberg, "Gap solitons in waveguide arrays," Phys. Rev. Lett. **92**, 093904 (2004).
35. B. Eiermann, T. Anker, M. Albiez, M. Taglieber, P. Treutlein, K. P. Marzlin, and M. K. Oberthaler, "Bright Bose-Einstein gap solitons of atoms with repulsive interaction," Phys. Rev. Lett. **92**, 230401 (2004).
36. C. M. Bender and S. Boettcher, "Real spectra in non-Hermitian Hamiltonians having PT symmetry," Phys. Rev. Lett. **80**, 5243–5246 (1998).
37. C. M. Bender, "Making sense of non-Hermitian Hamiltonians," Rep. Prog. Phys. **70**, 947–1018 (2007).
38. L. Feng, R. El-Ganainy, and L. Ge, "Non-Hermitian photonics based on parity-time symmetry," Nat. Photonics **11**, 752–762 (2017).

39. H. Zhao and L. Feng, "Parity-time symmetric photonics," Natl. Sci. Rev. **5**, 183–199 (2018).
40. S. K. Özdemir, S. Rotter, F. Nori, and L. Yang, "Parity-time symmetry and exceptional points in photonics," Nat. Mater. **18**, 783–798 (2019).
41. S. K. Gupta, Y. Zou, X.-Y. Zhu, M.-H. Lu, L.-J. Zhang, X.-P. Liu, and Y.-F. Chen, "Parity-time symmetry in non-Hermitian complex optical media," Adv. Mater. **32**, 1903639 (2020).
42. C. Hang, G. X. Huang, and V. V. Konotop, "PT symmetry with a system of three-level atoms," Phys. Rev. Lett. **110**, 083604 (2013).
43. Z. Zhang, Y. Zhang, J. Sheng, L. Yang, M.-A. Miri, D. N. Christodoulides, B. He, Y. Zhang, and M. Xiao, "Observation of parity-time symmetry in optically induced atomic lattices," Phys. Rev. Lett. **117**, 123601 (2016).
44. Z. H. Musslimani, K. G. Makris, R. El-Ganainy, and D. N. Christodoulides, "Optical solitons in PT periodic potentials," Phys. Rev. Lett. **100**, 030402 (2008).
45. J. Zeng and Y. Lan, "Two-dimensional solitons in PT linear lattice potentials," Phys. Rev. E **85**, 047601 (2012).
46. V. V. Konotop, J. Yang, and D. A. Zezyulin, "Nonlinear waves in PT-symmetric systems," Rev. Mod. Phys. **88**, 035002 (2016).
47. S. V. Suchkov, A. A. Sukhorukov, J. Huang, S. V. Dmitriev, C. Lee, and Y. S. Kivshar, "Nonlinear switching and solitons in PT-symmetric photonic systems," Laser Photon. Rev. **10**, 177–213 (2016).
48. J. Li, Y. Zhang, and J. Zeng, "Matter-wave gap solitons and vortices in three-dimensional parity-time-symmetric optical lattices," iScience. **25**, 104026 (2022).
49. Y. V. Kartashov, C. Hang, G. Huang, and L. Torner, "Three-dimensional topological solitons in PT-symmetric optical lattices," Optica **3**, 1048–1055 (2016).
50. B. I. Mantsyzov and R. N. Kuzmin, "Coherent interaction of light with a discrete periodic resonant medium," Zhurnal Eksperimentalnoi i Teoreticheskoi Fiziki **91**, 65–77 (1986).
51. D. E. Pelinovsky, *Localization in Periodic Potential: From Schrödinger Operators to the Gross-Pitaevskii Equation* (Cambridge University, 2011).
52. Z. J. Wong, Y. L. Xu, J. Kim, K. O'Brien, Y. Wang, L. Feng, and X. Zhang, "Lasing and anti-lasing in a single cavity," Nat. Photonics **10**, 796–801 (2016).
53. S. Longhi, "Optical realization of relativistic non-Hermitian quantum mechanics," Phys. Rev. Lett. **105**, 013903 (2010).
54. J. Yang, *Nonlinear Waves in Integrable and Nonintegrable Systems* (SIAM, 2010).